LA-UR-16-27359 (Accepted Manuscript)

Oxygen content tailored magnetic and electronic properties in cobaltite double perovskite thin films

Harrell, Zachary John
Enriquez, Erik M.
Chen, Aiping
Dowden, Paul Charles
Mace, Brennan
Lu, Xujie
Jia, Quanxi
Chen, Chonglin

To be published in: Applied Physics Letters

DOI to publisher's version: 10.1063/1.4977026

Permalink to record: http://permalink.lanl.gov/object/view?what=info:lanl-repo/lareport/LA-UR-16-27359

Oxygen Content Tailored Magnetic and Electronic Properties in Cobaltite Double Perovskite Thin Films

Zach Harrell[1,2], Erik Enriquez[1] Aiping Chen[1], Paul Dowden[1], Brennan Mace[2], Xujie Lü[1], Quanxi Jia[1,3,], Chonglin Chen[2,*]

[1] Center for Integrated Nanotechnology (CINT), Los Alamos National Laboratory, Los Alamos, NM 87545, USA

[2] Department of Physics and Astronomy, University of Texas at San Antonio, San Antonio, TX 78249, USA

[3] Department of Materials Design and Innovation, University at Buffalo - The State University of New York, Buffalo, NY 14260, USA

[*] Email: qxjia@buffalo.edu, cl.chen@utsa.edu

Keywords: thin films, magnetic and electronic properties, oxygen content

Abstract

Oxygen content in transition metal oxides is one of the most important parameters to control for desired physical properties. Recently, we have systematically studied the oxygen content and property relationship of double perovskite $PrBaCo_2O_{5.5+\delta}$ (PBCO) thin films deposited on $LaAlO_3$ (LAO) substrates. The oxygen content in the films was varied by in-situ annealing in a nitrogen, oxygen, or ozone environment. Associated with the oxygen content, the out-of-plane lattice parameter progressively decreases with increasing oxygen content in the films. The saturated magnetization shows a drastic increase and resistivity is significantly reduced in the ozone annealed samples, indicating the strong coupling between physical properties and oxygen content. These results demonstrate that the magnetic properties of PBCO

This manuscript was accepted by Appl. Phys. Lett. Click here to see the version of record.

films are highly dependent upon the oxygen contents, or the film with higher oxygen uptake has the largest magnetization.

Introduction

Functional transition metal oxide materials continue to be the subject of extensive research due to their interesting and important physical properties for a vast range of promising applications.[1] The interaction of the *3d*-orbitals in the transition metal atoms with the *2p*-orbitals of the oxygen atoms plays an important role in controlling functionalities. Especially, in perovskite oxides (ABO_3) with multiple possible valence states for the B-site cations, variations in oxygen content change the cation valence states at the B-site to balance the charge ($ABO_{3-\delta}$), leading to tunable physical properties in these materials.[2] The cation valence states of the B-site transition metals can also alter the overall oxygen stoichiometry and oxygen vacancy distribution, changing the oxygen stoichiometry to $O_{3-\delta}$.[3] In these materials, oxygen vacancies can significantly alter the crystal band structures and the spin-orbital interaction resulting in various anomalous electric and magnetic properties of transition metal oxides.[4,5] Especially, ordered oxygen vacancies can be formed in the families of cobalt and iron.[6] These vacancies result in the formation of long-range magnetic ordering and dramatically change the properties of the transition metal oxides.[7,8] Remarkably, functional properties in these systems, namely cobaltite and manganite perovskites, are extremely sensitive to oxygen content variation as changes in oxygen content (as little as $\delta = 0.01$) can have immense effect on transport properties.[9] Recent researches indicate that the ordered oxygen vacancy structure can significantly enhance oxygen ion transport in these materials.[10,11] Additionally, cobaltite perovskites show various interesting magnetic properties and electronic transport properties as the Co-O-Co chains allow for ferromagnetic and antiferromagnetic ordering, as well as metallic,

This manuscript was accepted by Appl. Phys. Lett. Click here to see the version of record.

semiconducting, or insulating transport behavior.[12] $PrBaCo_2O_{5.5+\delta}$ (PBCO) bulk/powder double perovskite has been shown to alter its magnetic and electronic transport properties significantly based on oxygen content and annealing condition, for example, PBCO thin films exhibit reduced defect concentration when treated to an oxygen anneal *vs*. no anneal.[13] Garcia-Munoz *et al.* and Ganorkar *et al.* showed that for $\delta > 0.2$, PBCO undergoes a paramagnetic-to-ferromagnetic-to-antiferromagnetic ordering with decreasing temperature.[14,15] In addition, a slow cooling process (1.67°C/min) following synthesis results in increased oxygen uptake and enhanced magnetic properties.[16] It is clear that optimization of oxygen content is crucial in obtaining desired properties in complex oxides. The oxygen content in materials like PBCO is normally adjusted by post annealing treatments in different chemical environments.

PBCO thin films were studied not only for their sensitivity to oxygen content in the lattice, but also because PBCO shows a nearly optimal composition among lanthanide cobaltite double perovskites for A-site (Pr, Ba) ordering as well as for oxygen vacancies to reside in the PrO layers.[19] Thus it is feasible to minimize extraneous effects in the lattice to better understand the specific role of increased oxygen uptake. Usually, the samples are typically held at elevated temperatures in oxygen and then slowly cooled over many hours or even days to approach fully oxygenated samples with O_6 in the double perovskite structure, or alternatively subject to extended post annealing treatments in most reports.[20,21] However, in many transition metal oxides, the metal atom ligand sites are occupied by single oxygen atoms, rather than diatomic oxygen. This means that the diatomic oxygen must first overcome an energy barrier to dissociate into oxygen ions before it can diffuse into the oxygen vacancies, as shown in similar perovskite materials.[10] In this study, we have focused on enhancing magnetic and electronic properties of PBCO epitaxial thin films by tuning the oxygen content via *in-situ* annealing in oxygen deficient,

oxygen rich, and ozone rich environments. By using flowing ozone gas during annealing, we take advantage of the decomposition at elevated temperature of the O_3 molecule in the deposition chamber, allowing for reactive O to enter the lattice without first dissociating as O_2.

Results and Discussion

Figure 1 shows the X-ray and RSM data. The lower inset shows the diffraction pattern from 20° to 50°, for ozone, oxygen, and nitrogen annealed samples, indicating that the films are (00*l*) oriented. Analysis yields out-of-plane lattice parameters of 7.726 Å, 7.720 Å, and 7.715 Å for the films treated in nitrogen, oxygen, and ozone, respectively. Additionally, Reciprocal Space Mapping (RSM) scans were conducted for these films around the (103) LAO peaks (corresponding to (106) for PBCO, the RSM for the film annealed in ozone is included in the upper inset). LAO substrates were chosen such that film relaxation begins at a small critical thickness to minimize interface strain contribution effects on magnetic and electronic properties.[22] Bulk PBCO exhibits pseudocubic *a/b* axis lattice parameters of approx. 3.93 Å, with a doubled *c*-axis parameter of approx. 7.655 Å, typical of the '112' double perovskites (where the ratio of *a*:*b*:*c* axis lattice parameters is approximately 1:1:2). This yields about a 3.693% (compressive) in-plane mismatch on LAO. A thin strained interfacial layer is evident in the RSM scan of the PBCO film as the (106) peak is elongated in Q_x which is expected at our estimated thickness of 150 nm. The relaxed region is the higher intensity area marked by the dashed circle. The in-plane lattice parameter for the ozone annealed sample is determined to be 3.902 Å based on the RSM scan, consistent with the reduction of the *a*/*b* lattice parameters with out-of-plane elongation. The oxygen and nitrogen annealed samples have in-plane lattice parameters of 3.916 Å and 3.900 Å, respectively. Interestingly, the oxygen annealed sample shows an increased lattice parameter compared to the nitrogen and ozone annealed samples. This could be due to the

This manuscript was accepted by Appl. Phys. Lett. Click here to see the version of record.

emergence of an orthorhombic distortion that can be found in bulk samples near $O_{5.5}$, where the *a*-axis parameter exhibits a "hump" like behavior with a maximum near $O_{5.5}$ and decreasing with either more or less oxygen in the lattice.[23] In comparison with bulk PBCO, all PBCO films in this study show an increased out-of-plane lattice parameter, possibly resulting from the oxygen deficiency. Alternatively, the increased out-of-plane lattice parameters might result from some residual strain remaining in the film. As the PBCO film and LAO substrate cool from the annealing process, differing coefficients of thermal expansion may cause the film and substrate lattices to contract at different rates, resulting in a partially strained film at room temperature. Since the film thicknesses are over 12 times the estimated critical thickness of 12.3 nm, the interface strain should be mostly relaxed, however some partial strain remains as discussed previously. As the temperature, laser energy, repetition rate, etc. were the same for each film, the dominant cause for the variation in lattice parameter as determined by XRD/RSM is directly related to the variation in oxygen content across the three annealing treatments. The RSM scans shown in Figure S1 exhibit subtly decreasing film peak widths from nitrogen to ozone annealed samples, characteristic of reduced defect concentration or possibly decreased octahedral distortion or mosaicity. The reduction in out-of-plane lattice parameter with increasing oxygen content is confirmed in several other thin film perovskites, including variation of unit cell volume due to B-site transition metal cation valence change as a possible mechanism.[24,25] A fully oxidized PBCO thin film ($PrBaCo_2O_6$) will have cobalt in an average valence state of +3.5, from equal parts of mixed valence Co^{3+}/Co^{4+}. As a result of reduced oxygen content toward $O_{5.5}$, the cobalt atoms all tend toward Co^{3+} causing the lattice to expand as cobalt and most other transition metal atoms increase ionic radius as their valence is reduced. Therefore, the PBCO peak shifts higher in Q_z from nitrogen to oxygen to ozone, again indicating increased oxygen uptake in each successive case.

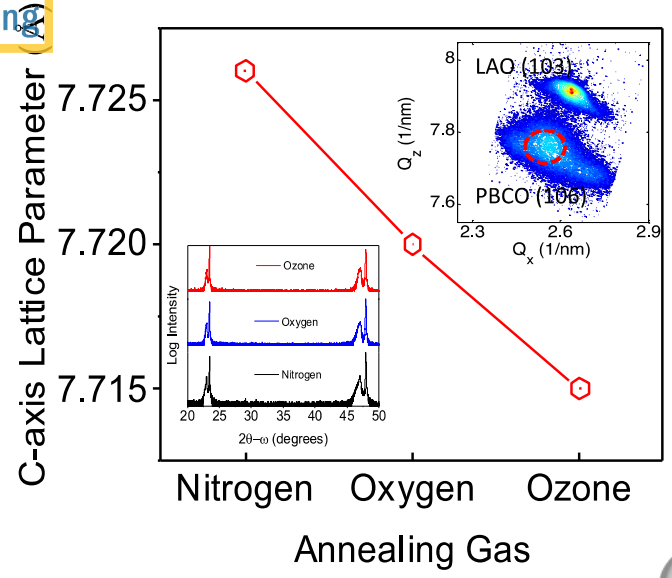

magnetization *vs.* applied magnetic field (*M-H*) measured at 10 K. *M-T* and *M-H* data were collected with the field applied in the film plane due to the *a*/*b* axes being the "easy axis" for lanthanide cobaltite perovskites' magnetic order and electronic conductivity.[26] Figure 2(a) is the zero-field cooled (ZFC) *M-T* curves for each different anneal environment. Strikingly, the ozone annealed sample shows a nearly 400% increase in peak magnetization over the oxygen annealed sample and a greater than 2500% increase over the nitrogen annealed sample in these curves. The ZFC curves show an onset of ferromagnetic (FM) ordering at about 175 K which quickly collapses as competing antiferromagnetic (AFM) regimes begin to dominate at lower temperatures. This type of behavior is also seen in other $LnBaCo_2O_{5.5+\delta}$ thin films (Ln = La, Pr, Nd, etc.) and is typical of a cluster glass behavior consisting of competing domains of FM and

This manuscript was accepted by Appl. Phys. Lett. Click here to see the version of record.

AFM regions.[21,22] The field-cooled scans in Figure 2(b) also show quite interesting behavior. All samples show onset of FM order at approx. 175 K, however the nitrogen and oxygen annealed samples may show some slight onset of AFM behavior as evidenced by the decrease in magnetization near 100 K. During cooling, this PM-FM-AFM transition is characteristic of bulk PBCO samples with oxygen content near $O_{5.5}$ to $O_{5.75}$, although there is some disagreement on what oxygen content exactly relates to this behavior.[14,16] Most interestingly, the onset of AFM ordering is absent in the ozone annealed sample, giving indirect evidence of elevated oxygen content. Although there is some variance in the range of oxygen content that yields this behavior, evidence points to oxygen content of at least $O_{5.65}$, but possibly as high as $O_{5.85}$.[15] In order to confirm that increased oxygen content modifies the metal-oxygen interaction mainly in the "easy axis" or *a/b* plane, we measured in-plane and out-of-plane *M-H* hysteresis loops. The hysteresis loop of the film annealed in ozone in Figure 2(c) exhibits stronger ferromagnetic response than that of the films annealed in oxygen and nitrogen. This can be related to how the oxygen content can influence the crystal field splitting and affect the spin state of the cobalt atoms. As discussed above, oxygen vacancies can change the valence or oxidation state of the cobalt atoms, resulting in a re-distribution of electrons according to the energy of the crystal field splitting. Depending on how the crystal field energy changes due to the oxygen vacancy, it may be energetically favorable for previously unpaired electrons to begin to pair up and reduce the spin state of cobalt. Depending on the magnitude of the splitting energy, it may be possible for electrons to thermally re-distribute into a higher spin state, however no such transition is evident in the data presented here, as the increasing temperature only serves to overall reduce the magnetic response in all samples. Figure 2(d) compares the in-plane and out-of-plane *M-H* loops for ozone annealed samples. We consider that the magnetic "easy axis" is in the plane of the film due to the

tendency of oxygen vacancies to reside in the PrO_{δ} planes rather than the CoO_2 or BaO planes.[15,21] Oxygen vacancies along the *c*-axis of the film will disrupt the double/superexchange interaction in the out-of-plane direction that is responsible for magnetic ordering, resulting in magnetic anisotropy from the reduced magnetic response along the *c*-axis direction as shown in other Lanthanide double perovskite materials.[27,28] Furthermore, the magnetic anisotropy can typically be attributed to strain, magnetocrystalline effects, or shape.[29] While the film near the interface is still fully strained, the film is significantly thicker than the estimated critical thickness as mentioned previously. As a result, strain from the film-substrate interface should not be a dominant parameter in the films' magnetic properties. By the same reasoning, the magnetocrystalline anisotropy contributions might play a role as the films have an increased out-of-plane lattice parameter as compared to bulk. In this case the increased lattice parameter is again attributed to oxygen deficiency. Additionally, the shape anisotropy energy ($2\pi M^2$, where M is the saturated magnetization) coupled with the oxygen vacancies along the *c*-axis distorts the out-of-plane *M-H* loop and results in an in-plane easy axis.[29,30]

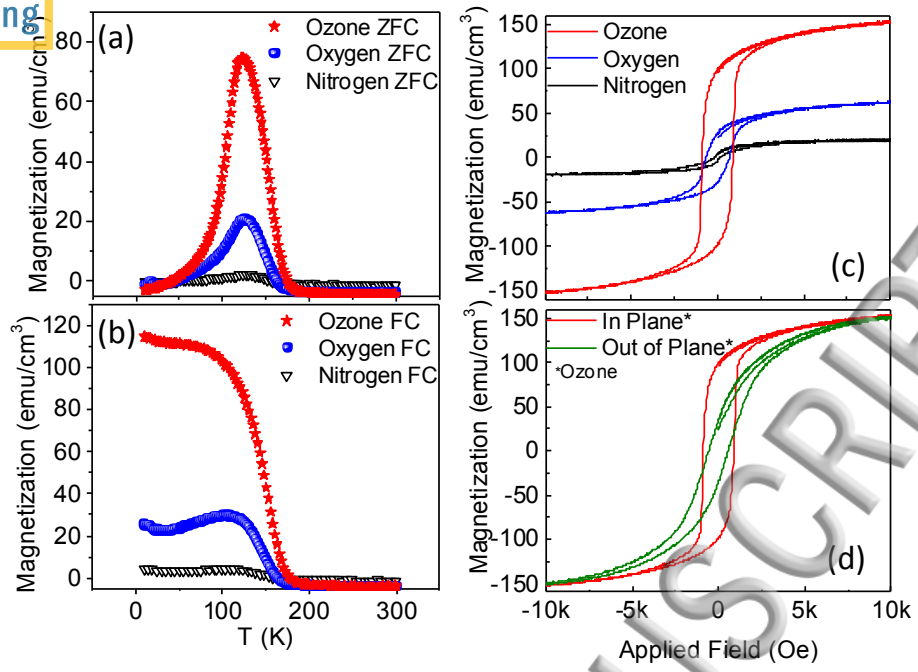

Figure 2. Magnetic properties of each anneal type. (a) PBCO ZFC in-plane *M-T* curves in 500 Oe field, (b) PBCO FC in-plane *M-T* curves in 500 Oe field, (c) In-plane *M-H* hysteresis loops at 10 K for each anneal environment, and (d) in-plane *vs*. out-of-plane *M-H* loops for ozone sample only measured at 10 K.

In addition to magnetic properties, oxygen content has significant influence on the electrical transport properties of PBCO thin films as well. Figure 3 shows as-measured resistivity data as a function of temperature. The samples all display typical semiconductor/insulator behavior as resistivity (ρ) decreases with increasing temperature. Surprisingly, there is very small difference between the oxygen and nitrogen annealed curves, however the ozone annealed PBCO sample shows a dramatic reduction in resistivity over the other two samples. Resistivity values at 150 K for the films annealed in nitrogen, oxygen, and ozone are 46.669 Ω-cm, 45.807 Ω-cm, and 6.199 Ω-cm respectively.

This manuscript was accepted by Appl. Phys. Lett. Click here to see the version of record.

Figure 3(a) depicts a typical Arrhenius fitting, often applied to semiconducting materials to determine their activation energy or band gap. The equation is reproduced here:

$$\rho(T) = A \exp\left(\frac{E_a}{kT}\right) \quad (1)$$

where E_a is the activation energy or gap energy, k is the Boltzmann constant given in units of eV/K, and T is temperature in K. It is obvious due to the non-linearity of the ln(ρ) *vs.* $1/T$ fit that this data cannot be completely fit by the Arrhenius model as the fitting is accurate for higher temperatures but diverges considerably below approx. 200 K, probably due to the local charge disordering and/or interface strain in these samples. Although the Variable Range Hopping model is often used to describe disordered systems, it has seen some success in describing complex oxide semiconductors/insulators at low temperatures and even superconducting oxides above their critical temperatures.[22,31] The general equation for this model is given below as presented by Mott[32]:

$$\ln(\sigma) = A - \frac{B}{T^{1/4}} \quad (2)$$

where A and B are material dependent constants relating to the Fermi level and average electron hopping energy or range. In terms of resistivity, this model typically requires a ln(ρ) *vs.* $T^{1/4}$ fitting in $LnBaCo_2O_{5.5+\delta}$ materials as the exponent on T can assume different values based on the system it describes.[31] As seen in Figure 3(b) this model fits the data reasonably, supporting its use to describe low temperature transport in cobaltite double perovskites, where charge carriers (along Co – O – Co chains) are typically localized. Interestingly, the VRH model fits the high temperature region very well in addition to the Arrhenius model. At these higher temperatures, we potentially have a mix of conduction mechanisms with thermal conduction

This manuscript was accepted by Appl. Phys. Lett. Click here to see the version of record.

becoming dominant as temperatures continue to rise. This may result from the effect of thermal expansion difference and interface strain between the films and substrates.[33] Thus, at high temperature the Arrhenius model becomes the "good fit", which enables one to determine the activation energy from the slope of the fit line. Toward lower temperatures, due to the different thermal expansive coefficients, regions of local charge disordering may be formed. This can be seen from the linear fit divergence. Therefore, the VRH model becomes dominant, and a "crossover" temperature to transition between models is emergent. Table SI (see supplemental information) summarizes these values as well as many other critical values presented above. In addition to the lower resistivity in the ozone annealed samples, we see a lower activation energy in the Arrhenius fit, as expected. In the VRH model, the slope of the fit is tied to the "hopping energy" required for a charge carrier to move between states. The ozone annealed sample shows the smallest slope and thus requires a lower hopping energy resulting in reduced resistivity. When it is applied to the as-measured resistivity data in Figure 3, the oxygen and nitrogen annealed samples show similar resistivities, indicating that the nitrogen and oxygen annealed samples are similarly disordered but possess different oxygen contents. Thus, the key parameter to consider is the hopping energy necessary for charge transport. As the N_2 and O_2 annealed samples show similar hopping energies, this means that the hopping electrons can have similarly available possible hopping pathways. Since most oxygen vacancies tend to reside in the Pr-O plane of the unit cell (as discussed previously), the electron hopping energy can allow for farther than "nearest neighbor" conduction in the case of an oxygen vacancy. Additionally, even though a vacancy in the Pr-O_δ layer might leave the *a/b*-axis Co-O-Co conduction paths intact, those oxygen vacancies can change the valence state of the Co atom. As discussed previously, a defect of this type can not only change the Co-O bond length/angle, but also reduce the available charge

This manuscript was accepted by Appl. Phys. Lett. Click here to see the version of record.

carriers, and give a higher resistance state as the average Co valence tends toward integer values (3+/2+).[34]

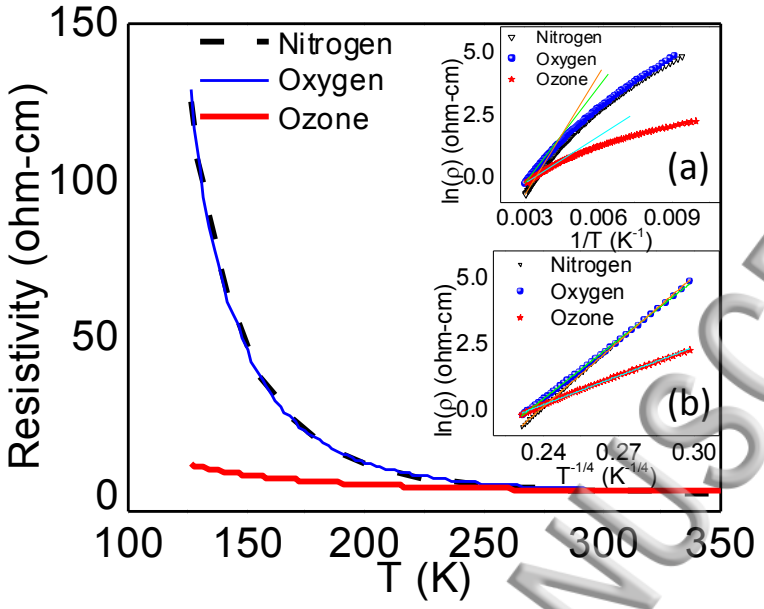

Figure 3. Resistance data and conduction model fittings, *R-T* plot, showing semiconducting/insulating behavior of all samples. (a) Arrhenius thermal activation model. Fit lines show divergence from this model at low temperatures. (b) Mott Variable Range Hopping model fitting shows excellent agreement with experimental data at all temperatures.

In summary, epitaxial PBCO thin films were deposited on LAO substrates via PLD. As in-situ annealing is a common treatment for complex transition metal oxide materials, we explored the effects of annealing gases (nitrogen, oxygen, and ozone) on the performance of the films. It was found that the out-of-plane lattice parameter progressively decreases with increased oxygen uptake in the films. Additionally, the magnetic and electronic properties showed drastically enhanced magnetic response as well as significantly reduced resistivity behavior in the ozone annealed samples. Our results agree well with measurements of various PBCO bulk/powder oxygen contents and support our claim of increased oxygen uptake during annealing. As all other

parameters remained the same, the addition of flowing ozone to a typical oxygen anneal requires no additional time over a traditional anneal, and can give equal or superior oxygen content to annealing techniques that require much longer time intervals.

See Supplementary Materials for detailed methods of thin film growth and characterization, additional RSM information, and magnetic ordering information.

Acknowledgements:

The work at Los Alamos National Laboratory was supported by the NNSA's Laboratory Directed Research and Development Program and was performed, in part, at the Center for Integrated Nanotechnologies, an Office of Science User Facility operated for the U.S. Department of Energy (DOE) Office of Science. Los Alamos National Laboratory, an affirmative action equal opportunity employer, is operated by Los Alamos National Security, LLC, for the National Nuclear Security Administration of the U.S. Department of Energy under contract DE-AC52- 06NA25396.

References:

[1] B. Raveau, J. Eur. Ceram. Soc. **25**, 1965 (2005).

[2] E. Enriquez, A. P. Chen, Z. Harrell, X. J. Lu, P. Dowden, N. Koskelo, M. Janoschek, C. L. Chen, Q. X. Jia, Appl. Phys. Lett. **109**, 141906 (2016).

[3] B. Raveau, Md. M. Seikh, *Cobalt Oxides: From Crystal Chemistry to Physics*. (Wiley-VCH Verlag & Co. KGaA, Weinheim, Germany, 2012).

[4] Y. Shuai, S. Zhou, D. Burger, H. Reuther, I. Skorupa, V. John, M. Helm, H. Schmidt, J. Appl. Phys. **109**, 084105 (2011).

[5] S. A. Lee, H. Jeong, S. Woo, J. Y. Hwang, S. Y. Choi, S. D. Kim, M. Choi, S. Roh, H. Yu, J. Hwang, S. W. Kim, W. S. Choi, Sci. Rep. **6**, 23649 (2016).

[6] W. Donner, C. L. Chen, M. Liu, A. J. Jacobson, Y. L. Lee, M. Gadre, D. Morgan, Chem. Mater. **23**, 984 (2011).

[7] K. Seema, R. Kumar, J. Supercond. Nov. Magn. **28**, 2735 (2015).

[8] V. V. Mehta, N. Biskup, C. Jenkins, E. Arenholz, M. Varela, Y. Suzuki, Phys. Rev. B **91**, 144418 (2015).

[9] Y. Fernandez-Diaz, L. Malavasi, M. C. Mozzati, Phys. Rev. B **78**, 144405 (2008).

[10] E. Enriquez, X. Xu, S. Bao, Z. Harrell, C. L. Chen, ACS Appl. Mater. Interfaces **7**, 24353 (2015).

[11] S. Bao, C. R. Ma, G. Chen, X. Xu, E. Enriquez, C. L. Chen, Y. Zhang, J. L. Bettis, Jr., M. H. Whangbo, C. Dong, Q. Zhang, Sci. Rep. **4**, 4726 (2014).

[12] C. Frontera, J. L. García-Muñoz, A. Llobet, M. A. G. Aranda, Phys. Rev. B **65**, 180405 (2002).

[13] Z. Yuan, J. Liu, C. L. Chen, C. H. Wang, X. G. Luo, X. H. Chen, G. T. Kim, D. X. Huang, S. S. Wang, A. J. Jacobson, W. Donner, Appl. Phys. Lett. **90**, 212111 (2007).

[14] J. L. Garcia-Muñoz, C. Frontera, A. Llobet, A. E. Carillo, A. Caneiro, M. A. G. Aranda, M. Respaud, C. Ritter, E. Dooryee, JMMM **272-276, Part 3**, 1762 (2004).

[15] S. Ganorkar, K. R. Priolkar, P. R. Sarode, A. Banerjee, R. Rawat, S. Emura, J. Phys.: Condens. Matter **24**, 476003 (2012).

[16] X. Zhang, X. M. Wang, H. W. Wei, X. H. Lin, C. H. Wang, Y. Zhang, C. Chen, X. P. Jing, Mater. Res. Bull **65**, 80 (2015).

[17] J. Liu, G. Collins, M. Liu, C.L. Chen, J. He, J. Jiang, and E. I. Meletis, Appl. Phys. Lett. **100**, 193903 (2012).

[18] M. Liu, S. P. Ren, R. Zhang, Z. Xue, C. R. Ma, M. Yin, X. Xu, S. Y. Bao, and C. L. Chen, Sci. Rep. **5**, 10784 (2015).

[19] H. Yamada, M. Kawasaki, Y. Tokura, Appl. Phys. Lett. **80**, 622 (2002).

[20] M. Liu, C. R. Ma, J. Liu, G. Collins, C. L. Chen, J. Hie, J. Jiang, E. I. Meletis, L. Sun, A. J. Jacobson, M. H. Whangbo, ACS Appl. Mater. Interfaces **4**, 5524 (2012).

[21] S. Streule, A. Podlesnyak, J. Mesot, M. Medarde, K. Conder, E. Pomjakushina, E. Mitberg, V. Kozhevnikov, J. Phys.: Condens. Matter **17**, 3317 (2005).

[22] C. R. Ma, M. Liu, J. Liu, G. Collins, Y. M. Zhang, H. B. Wang, C. L. Chen, Y. Lin, J. He, J. C. Jiang, E. I. Meletis, A. J. Jacobson, ACS Appl. Mater. Interfaces **6**, 2540 (2014).

[23] S. Ganorkar, K. R. Priolkar, P. Sarode, A. Banerjee, J. Appl. Phys. **110**, 053923 (2011).

[24] A. P. Chen, F. Khatkhatay, W. Zhang, C. Jacob, L. Jiao, H. Wang, J. Appl. Phys. **114**, 124101 (2013).

[25] C. Wang, B. L. Cheng, S. Y. Wang, H. B. Lu, Y. L. Zhou, Z. H. Chen, G. Z. Yang, Thin Solid Films **485**, 82 (2005).

[26] Z. X. Zhou, S. McCall, C. S. Alexander, J. E. Crow, P. Schlottmann, S. N. Barilo, S. V. Shiryaev, G. L. Bychkov, R. P. Guertin, Phys. Rev. B **70**, 024425 (2004).

[27] M. M. Seikh, C. Simon, V. Caignaert, V. Pralong, M. B. Lepetit, S. Boudin, B. Raveau, Chem. Mater. **20**, 231 (2008).

[28] A. A. Taskin, A. N. Lavrov, Y. Ando, Phys. Rev. B **71**, 134414 (2005).

[29] A. P. Chen, J. M. Hu, P. Lu, T. Yang, W. Zhang, L. Li, T. Ahmed, E. Enriquez, M. Weigand, Q. Su, H. Wang, J. X. Zhu, J. L. MacManus-Driscoll, L. Q. Chen, D. Yarotski, Q. X. Jia, Sci. Adv. **2,** e1600245 (2016).

[30] A. P. Chen, N. Poudyal, J. Xiong, J. P. Lu, Q. X. Jia, Appl. Phys. Lett. **106**, 111907 (2015).

[31] Z. Celik-Butler, Solid State Electron. **41**, 6 (1997).

[32] N. F. Mott, Philosophical Magazine **19**, 835 (1969).

[33] Y. Lin, C. L. Chen, J. Mat. Sci. **44**, 5274 (2009).

[34] S. Y. Bao, C. R. Ma, G. Chen, X. Xu, E. Enriquez, C. L. Chen, Y. M. Zhang, J. L. Bettis, M. H. Whangbo, C. Dong, Q. Y. Zhang, Sci. Rep. **4**, 5 (2014).